

Nano-antibiotics combined with laser irradiation to reduce the development of drug resistance of *K. Pneumoniae* and accelerate wound healing

Tiansheng Liu¹, Guowei Zhong², Dongying Tang², Xu Liu³, Xianghua Zhong¹, Yuejun Yang¹, Chunyi Tong², and Xiaoping Yang¹

¹Hunan Normal University

²Hunan University

³Hunan University of Chinese Medicine

February 22, 2024

Abstract

Bacterial infections, especially infections caused by multi-drug resistant bacteria, pose a serious threat to human health and bring huge challenges to clinical treatment. The excessive use of antibiotics can easily lead to the emergence of bacterial resistance, which severely limits clinical treatment options. There is an urgent need to develop high-efficiency antibacterial materials and treatment strategies to inhibit infections caused by multidrug-resistant bacteria. In this work, a nanocomposite named Ofloxacin@HMPB@HA(OHH NPs) combined with the laser irradiation was used to reduce the development of drug resistance and accelerate wound healing in a model infected by *Klebsiella pneumoniae*(*K.Pneumoniae*). In vitro results showed that compared with OHH NPs or NIR laser irradiation alone, this combination strategy can exert a synergistic effect on anti-*K.Pneumoniae* by destroying cell integrity with generating ROS and reducing ATP, and also inhibit the development of bacterial resistance. Moreover, in vivo experiments have shown that the system effectively promotes wound healing through killing *K.Pneumoniae* and promoting the formation of new tissues. In summary, these results indicate that OHH NPs show great potential in the clinical application of bacterial infections.

Nano-antibiotics combined with laser irradiation to reduce the development of drug resistance of *K. Pneumoniae* and accelerate wound healing

Tiansheng Liu^{1#}, Guowei Zhong^{2#}, Dongying Tang², Xu Liu³, Jialong Fan², Xianghua Zhong¹, Yuejun Yang^{1*}, Chunyi Tong^{2*}, Xiaoping Yang¹

1 School of Medicine, Key Laboratory of Protein Chemistry and Developmental Biology of Fish of Ministry of Education, Hunan Normal University, Changsha, 410125, PR China.

2 College of Biology, Hunan University, Changsha, 410082, PR China

3 School of Pharmacy, Hunan University of Chinese Medicine, Changsha 410208, China

These authors contributed to the work equally and should be regarded as co-first authors.

* To whom correspondence should be addressed.

Abstract

Bacterial infections, especially infections caused by multi-drug resistant bacteria, pose a serious threat to human health and bring huge challenges to clinical treatment. The excessive use of antibiotics can easily lead

to the emergence of bacterial resistance, which severely limits clinical treatment options. There is an urgent need to develop high-efficiency antibacterial materials and treatment strategies to inhibit infections caused by multidrug-resistant bacteria. In this work, a nanocomposite named Ofloxacin@HMPB@HA(OHH NPs) combined with the laser irradiation was used to reduce the development of drug resistance and accelerate wound healing in a model infected by *Klebsiella pneumoniae*(*K.Pneumoniae*) . In vitro results showed that compared with OHH NPs or NIR laser irradiation alone, this combination strategy can exert a synergistic effect on anti-*K.Pneumoniae* by destroying cell integrity with generating ROS and reducing ATP, and also inhibit the development of bacterial resistance. Moreover, in vivo experiments have shown that the system effectively promotes wound healing through killing *K.Pneumoniae* and promoting the formation of new tissues. In summary, these results indicate that OHH NPs show great potential in the clinical application of bacterial infections.

Keywords

Hollow Mesoporous Prussian Blue, antibiotic resistance, antibacterial nanoplatform, photothermal therapy

Introduction

Over the past decades, the ever-growing emergence of bacterial infections causes devastating consequences to public health worldwide¹. Clinically, the most widely employed and effective therapeutic method of bacterial infections is antibiotics treatment²⁻³. However, the overuse of antibiotics has given rise to the appearance of multidrug-resistant (MDR) bacteria which weakens the effectiveness of most antibiotics⁴. Moreover, high-dose antibiotics treatment has great potential to induce severe adverse effects and systemic toxicity such as angioedema, thrombophlebitis, anaphylactic shock and so on⁵⁻⁶. Thus, there is an urgent requirement for development of new effective antibacterial strategies which make rational use of conventional antibiotics and minimize antibiotic dose.

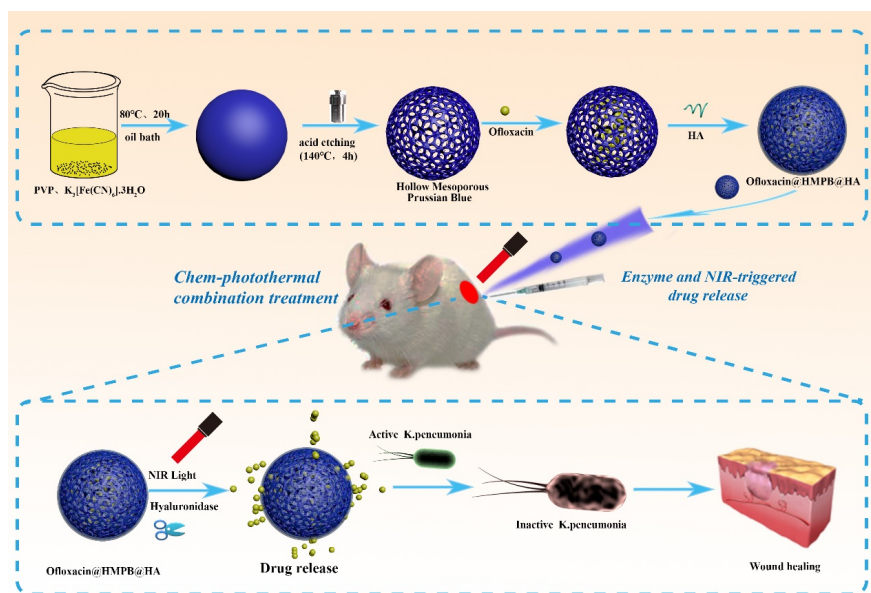
Recently, nanoparticle (NP)-based local “on-demand” antibacterial drugs delivery systems have received burgeoning attention since they can prolong drugs retention at the infected area with low undesired drugs diffusion, improved therapeutic efficacy and reduced toxicity⁷⁻⁹. For instance, Gu and co-workers reported levofloxacin hydrochloride-loaded, silver core-embedded mesoporous silica for synergistically combating drug-resistant bacterial infections¹⁰; Wu and co-workers developed ciprofloxacin-loaded photothermal PDA/GC hydrogel for combined chemo-photothermal therapy of bacterial infections¹¹; Han and co-workers successfully fabricated rifampicin-loaded endogenous stimulus-responsive liposome nanoreactors for a combined therapy of bacterial infections¹². Although NP-based drugs delivery systems can effectively enhance antibacterial efficacy and lower biological toxicity of antibacterial drugs, therapeutic effect of single modality of chemotherapy based on drugs delivery systems is still unsatisfactory due to poor diffusivity of drugs in targeted sites¹³, which will seriously hamper their practical applications in clinic. Chemotherapy-based synergistic therapy is a particularly encouraging strategy to strengthen the bactericidal effect for combating bacterial infections¹⁴.

Photothermal therapy (PTT) triggered by near-infrared (NIR) laser has been applied as one of the most effective antibacterial strategies¹⁵⁻¹⁶. PTT can cause bacterial death through hyperthermia-induced denaturation of bacterial enzymes and irreversible bacterial destruction¹⁷. Comparing with antimicrobials, this strategy presented many advantages for antibacterial application as follow: (1) NIR laser has high spatial resolution and a deep penetration ability to tissues with minimal invasiveness¹⁸; (2) PTT can efficiently kill bacteria in a short time (only a few minutes)¹⁹⁻²⁰; (3) PTT has broad-spectrum antibacterial ability and can efficiently eliminate MDR bacterial strains with less probability to induce drug resistance²¹; (4) NIR laser can focus on a targeted area to accelerate blood circulation with little influence on the whole body²²⁻²³. Unfortunately, the locally high temperature required to completely eradicate the bacteria may cause severe thermal injury to the surrounding healthy tissues²⁴. Combination of chemotherapy and PTT is an especially promising approach for overcoming the limitations of PTT alone.

To date, numerous nanomaterials have been developed as photothermal agents, including palladium NPs²⁵, carbon nanomaterials²⁶, black phosphorus²⁷, Au nanorods²⁸ and so on. Among these nanomaterials, Prus-

sian blue (PB) approved by USA Food and Drug Administration (FDA) as a clinical drug gains great popularity for PTT due to the eminent advantages of strong NIR radiation absorption ability, high photothermal efficiency, excellent chemical stability, splendid biocompatibility and low-cost²⁹⁻³⁰. More encouragingly, we have successfully prepared hollow mesoporous PB (HMPB) that has larger drug loading capacity owing to interior hollow cavity and more rough mesoporous surface compared with PB. Simultaneously, HMPB possess almost the same photothermal ability as PB. These unique features of HMPB make it an ideal photothermal agent as well as drug carrier, which can effectively combine chemotherapy and PTT³¹.

Herein, we fabricated a robust surface-adaptive, on-demand antibacterial nanoplatform by covering hyaluronic acid (HA) on ofloxacin loaded HMPB to exert the strong synergistic antibacterial effect involving antibiotic and PTT killing. As showed in Scheme 1, for the first time, we utilized the hyaluronic acid (HA)-modified HMPB as a nanocarrier to load the ofloxacin, a traditional antibiotic with broad spectrum of antibacterial property against both gram-positive and gram-negative bacteria, even MDR bacteria. HA with excellent biocompatibility was employed as the capping agent to prevent unwanted ofloxacin release in this system. Meanwhile, HA on the surface of HMPB acted in the role of “on-demand” releasing agent which can be degraded by hyaluronidase (HAase) secreted in numerous bacteria. The encapsulated ofloxacin could be released and further efficiently combat pathogenic bacteria at the infected area when the coating layer HA of the resulted OHH NPs was degraded by overexpressed HAase generated by bacteria. The intelligent behavior of “on-demand” release of this nanoplatform could considerably enhanced bioavailability of ofloxacin and reduced toxicity of ofloxacin. Additionally, under NIR light irradiation, the nanocarrier showed photothermal effect, which could generate locally increased temperature to inactivate bacteria. In summary, the OHH NPs exhibited surface-adaptive characteristic and on-demand synergistically antibacterial capability originated from the released ofloxacin and produced hyperthermia under NIR light irradiation, which could significantly improve the antibacterial efficacy and lowered the dosage of ofloxacin. Furthermore, this powerful antibacterial nanoplatform was successfully employed for the treatment of *K.pneumoniae* -infected wound.



2. Materials and Methods

2.1. Materials

$K_3[Fe(CN)_6] \cdot 3H_2O$ was brought from Fuchen Chemical Reagent Factory (China). Poly (N-vinylpyrrolidone)

(PVP) was obtained from Zhanyun Chemical Co., Ltd. (China). Ofloxacin, Haluronic acid and Polyacrylic acid were obtained from Macklin Biotechnology Co., Ltd (China). 1-(3-dimethylaminopropyl)-3-ethylcarbodiimide hydrochloride (EDC) and N-hydroxysuccinimide (NHS) were purchased from Sigma Aldrich. All other chemicals and solvents were of reagent grade.

2.2. Preparation of PBNPs.

PB NPs were synthesized according to the previous method developed by our group. In brief, 264 mg $K_3[Fe(CN)_6] \cdot 3H_2O$ and 3 g PVP were dissolved in 40 mL of 0.01 M HCl solution under stirring for 1 h at room temperature. Then, the mixture solution was heated at 80 °C for 20 h with oil bath. After centrifugation and water washing for 3 times, the precipitate was dried under vacuum for the preparation of PB NPs.

2.3 Preparation of HMPB NPs.

HMPB NPs were prepared following the previous method with little modification³². 100 mg PVP and 20 mg PB NPs were dissolved in 20 mL of 1 M HCl solution under magnetic stirring for 3 h. Then, the mixture solution was transferred into a stainless autoclave and heated at 140 °C for 4 h. After acid etching, HMPB NPs is collected by centrifugation and washed three times with deionized water.

2.4. Preparation of OHH NPs.

For synthesis of OHH NPs, 2 mg HMPB NPs and 2 mg ofloxacin were added to 1 mL of deionized water with stirring for 4 h. Then remove unbound ofloxacin by centrifugation. After centrifugation, 6 mg polyacrylic acid (PAA) was added into the mixture. Furthermore, the above solution was added 6 mg of EDC and 6 mg of NHS. After stirring for 2 h, 3 mg Haluronic acid (HA) was added into the mixed solution and further reacted overnight. Finally, OHH NPs were extracted by centrifugation.

2.5. Characterization of hybrids

SEM mapping, FTIR, X-ray diffraction (XRD) and X-ray photoelectron spectroscopy (XPS) were tested in Guangdong Puchuan Inspection Co, Ltd., China. UV–Vis absorption spectra were recorded with a UV-1800 spectrophotometer (Shimadzu, Japan). The hydrodynamic diameters and zeta potential of NPs were measured using a Zeta-sizer Nano ZS (Malvern, UK). The morphology of NPs was characterized by transmission electron microscope (TEM, JEM-2100F, JEOL).

2.6. Photothermal effect of OHH NPs

0.6 mL of PBS, HMPB NPs, ofloxacin or OHH NPs solution in Eppendorf tube was exposed to 808 nm NIR laser with a laser density of 1 W/cm² for 10 min. An infrared thermal camera was used to capture the infrared thermal images and record the real-time temperature every 20s. To assess the photostability of OHH NPs, the real-time temperature of OHH NPs (100 µg/mL) solution was recorded in five cycles with 5 min laser on and 10 min laser off.

2.7. In vitro antibacterial experiments

Methicillin-resistant *Staphylococcus aureus* (MRSA) and *K.pneumoniae* were cultivated separately overnight at 37 °C in Luria–Bertani broth (LB broth). The antibacterial effect of the nanomaterials was determined by the agar diffusion method. Briefly, 100 µL bacterial suspension (10⁸ CFU mL⁻¹) of MRSA or *K.pneumoniae* was spread homogeneously on the agar plate. Then, 25 µL of sample (PBS, HMPB NPs, ofloxacin and OHH NPs) dropped to a filter paper on MRSA and *K.pneumoniae* -coated agar plates. The agar plates were transferred into the 37 °C incubator. After incubation for 12 h, the diameters of inhibition area were measured to assess the bactericidal activity.

The plate counting method was adopted to test *in vitro* antibacterial efficiency of sample (PBS, HMPB NPs, ofloxacin and OHH NPs) combined with NIR laser irradiation. 200 µL of bacterial suspension (1 × 10⁴ CFU mL⁻¹) was incubated with PBS (control), HMPB, ofloxacin or OHH NPs and then irradiated with/without 808 nm laser at a power density of 1 W/cm² for 5 min. Afterwards, 100 µL of appropriately diluted bacterial

suspension was spread on LB agar plate followed by incubated at 37°C for 24 h. Bacterial colony forming units were counted and antibacterial efficiency was calculated according to the following equation:

$$\text{Survival ratio (\%)} = \text{CFU}_{\text{sample}}/\text{CFU}_{\text{control}} \times 100\%$$

2.8. Live/dead staining and ROS detection assays

The bacterial viability was investigated using Live/Dead Bacterial Viability Kit. *K.pneumoniae* after different treatments was collected by centrifuging (8000 rpm, 5 min) and then co-dyed with Calcein-AM and propidium iodide (PI) in dark for 30 min. After that, the bacteria were washed with normal saline to remove excess dye. Finally, bacterial solutions were dropped on the glass slides and imaged Confocal Microscope (FV1200, Olympus).

For the analysis of intracellular ROS content, 10^8 CFU mL⁻¹ *K.pneumoniae* cells were added into the PBS (control), HMPB (100 µg/mL), ofloxacin (10 µg/mL), and OHH NPs (100 µg/mL) and further incubated for 30 min, the net concentration of the HMPB substrate in all sample groups has been maintained at 100 µg/mL. After that, the *K.pneumoniae* cells were rinsed with medium and stained with DCFH-DA under 37 °C for 20 min and then analyzed using a confocal microscope (FV1200, Olympus). Quantitative determination of the ROS content in the cell samples was further carried out as a complement to the characterizations above.

2.9. Morphological study of bacteria

The *K.pneumoniae* cells treated by different samples were collected after centrifugation (8000 rpm, 5 min) and rinsed three times with normal saline. Thereafter, the treated bacteria were fixed with 2.5% glutaraldehyde solution in dark for 4 h at 4 °C. Subsequently, the fixed samples were dehydrated for 10 min with sequential concentrations (30%, 50%, 70%, 80%, 90%, 95% and 100%) of ethanol solution, respectively, followed by observing under a scanning electron microscope.

2.10. ATP assay

The metabolic activity of bacteria was assessed by an Enhanced ATP Assay Kit (Beyotime). *K.pneumoniae* cells treated with different samples was harvested by centrifuging (8000 rpm, 5 min) at 4 °C and resuspended in 100 µL of lysis buffer. Subsequently, all samples were transferred into an ultrasonic cell disruption instrument at 30% power (3 s on, 5 s off) for 5 min in an ice bath. Finally, the harvested supernatant was determined on a multi-mode detection platform in luminance mode.

2.11. Protein leakage study

Protein leakage detection of bacteria was performed referring to our previous method. In brief, 10^8 CFU mL⁻¹ *K.pneumoniae* was firstly incubated with PBS (control), HMPB (100 µg/mL), ofloxacin (10 µg/mL), and OHH NPs (100 µg/mL) for 12 h at 37 °C. Hereafter, bacterial suspension of *K.pneumoniae* was centrifuged at 8000 rpm for 5 min at 4 °C and the harvested supernatant was immediately transferred into a 96-well plate. The concentration of protein was determined using a BCA Protein Assay Kit (Cat#PC0020, Solarbio).

2.12. In vitro antibiofilm assay

For establishment of biofilms, 5×10^8 CFU mL⁻¹ of *K.pneumoniae* cells were added to 96-well plate (100 µL per well) and incubated under stationary conditions at 37 °C for 1 day. After biofilm formation, the medium was discarded and the plates were washed with PBS to remove the planktonic bacteria. Then 200 µL of HMPB (100 µg/mL), ofloxacin (10 µg/mL) and OHH NPs with HMPB concentration of 100 µg/mL was added to the plates, respectively. For control group, 200 µL of PBS without nanomaterials was used. All groups were incubated at 37°C for 12 h. For the NIR irradiated group, 808 nm laser at power density of 1 W/cm² was used to illuminate sample for 5 min. The media in each well was then removed, and the plates were washed carefully with PBS one time. The biofilm in each well was fixed with methanol for 15 min and stained with 0.1% crystal violet for 15 min. After washing with Milli-Q water for three times, ethanol (100 µL per well) was added to solubilize the crystal violet staining. OD₅₆₀ in each well was read to determine the biofilm formation.

Additionally, to obtain the 3D morphology of the *K.pneumoniae* biofilms, the biofilms formed under different treatments was dyed by propidium iodide (PI) for 30 min in the dark. After, the biofilms stained by PI were washed three times with PBS and observed by a confocal laser scanning microscope (FV1200, Olympus). The red fluorescence intensity of 3D images of biofilms was quantified using Image J.

2.13. Ofloxacin release behavior

The measurement and calculation methods are based on our previous reports³³. Briefly, 1 mL of OHH NPs solution with the concentration of 100 $\mu\text{g}/\text{mL}$ with/without HAase was irradiated by 808 nm NIR laser at power density of 1 W/cm^2 for 5 min. Then, 200 μL of solution was taken out every 30 min and the solution was immediately centrifuged at 13,000 rpm for 10 min. Finally, the concentration of ofloxacin of the supernatant was measured by UV-Vis spectrophotometer. The drug loading capacity and entrapment efficiency of the OHH NPs were calculated as follows:

$$\text{Loading capacity (\%)} = (M_T - M_U) / M_P \times 100 \%$$

where M_T represents the total mass of drug, M_U represents the mass of the unencapsulated drug, and M_P represents the mass of PB and HMPB.

2.14. In vitro cytotoxicity assay

To investigate the *in vitro* cytotoxicity of different nanomaterials, NIH-3T3 and HUV-EC cells (1×10^4) were seeded in a 96-well plate. After incubation for 24 h, the culture media was removed and fresh culture media comprising different concentrations of HMPB, ofloxacin or OHH NPs (0, 25, 50, 75, 100, 125 $\mu\text{g}/\text{mL}$). After 24 h incubation, the samples were washed with PBS three times and 100 μL of CCK-8 solution was added into each well. After incubation for 2 h, cell viability was measured by a microplate reader in the absorbance of 450 nm.

Hemolysis assay was performed using fresh Balb/c mouse blood. The fresh mouse blood cells were harvested after centrifugation (3500 rpm, 5 min, 4 °C). After that, 950 μL of PBS containing various concentrations of nanomaterials are mixed with 50 μL of red blood cells. After incubation for 2 h at 37 °C, the samples were centrifuged (3500 rpm, 5 min, 4 °C) and the optical density at 540 nm of the supernatant were determined on a microplate reader. Each sample was measured in triplicate. PBS and pure water were acted the role of a negative and positive control. The ratio of hemolysis was calculated using the following equation:

$$\text{Hemolysis (\%)} = (A_{\text{sample}} - A_{\text{negative}}) / (A_{\text{positive}} - A_{\text{negative}}) \times 100\%;$$

Where A_{sample} is the absorbance value of the supernatant after the addition of HMPB, ofloxacin and OHH NPs, respectively. A_{negative} and A_{positive} are the absorbance values after the addition of PBS and pure water, respectively.

2.15. In vivo treatment of wound infection in Balb/c mice

All procedures for animals were approved by the Institutional Animal Care and Use Committee of Hunan University. Six-week-old female Balb/c mice were obtained from Hunan SJA Laboratory Animal Co., Ltd. (Changsha, China). *K.Pneumoniae* was used as bacterial strain to infect mice. All mice were randomly divided into five groups: PBS group, HMPB group, ofloxacin group, OHH group and OHH+NIR group. A circular skin wound (diameter of 10 mm) was prepared on the backbone of mice. Then, 100 μL of *K.pneumoniae* suspension (10^8 CFU mL^{-1}) was dropped on circular wounds for mouse infection. Three days after continuous infection, 100 μL of PBS, HMPB, ofloxacin OHH was smeared on the surface of the wounds every 2 days with the same antibiotic concentration (10 μg mL^{-1}) and the same HMPB concentration (100 μg mL^{-1}), respectively. The OHH+NIR group was irradiated by 808 nm NIR laser (1 W/cm^2) for 5 min. Meanwhile, the diameter of the wounds was measured and the wounds were photographed every 2 days.

On the 12th day, all mice were euthanized, and skin tissues and major organs were excised to study their healing efficiency and biological safety *in vivo*, respectively. In order to evaluate the antibacterial effect in

vivo, these infected tissues were also collected for coating assay. Collect blood for measuring biochemical indicators.

2.17. Statistical analysis

Each data was expressed as mean \pm standard deviation, and each experiment is performed at least 3 times. Tukey's post-test was used for one-way analysis of variance (ANOVA) for analysis. Among them, * $P < 0.05$, ** $P < 0.01$, *** $P < 0.001$, the difference between different groups is considered to be statistically significant.

3. Results and discussion

3.1. Preparation and characterization of OHH NPs

The synthesis method of OHH NPs was schematically illustrated in Scheme 1. The morphology of the obtained nanomaterials was characterized through transmission electron microscopy (TEM). The image of Fig. 1A indicated that PB NPs was successfully prepared with a size of 100 nm^{32, 34-36}. HMPB NPs were synthesized on basis of PB NPs by the controllable acid etching strategy, accompanying with morphological change from square to spheric. Fig. 1B clearly showed hollow mesoporous Prussian blue (HMPB) were successfully prepared with a diameter of 75 nm and the hollow mesoporous structure. After loading ofloxacin and coating with HA, the uniform size of OHH NPs slightly increased to 78 nm (Fig. 1C), which was consistent with the result of the dynamic light scattering (Fig. 1D). In Fig. 1E, the zeta potential of HMPB increased from -19 mV to 8 mV after loading ofloxacin owing to the positive charge of ofloxacin, while HA coating layer with a negative charge caused the decrease of HMPB loaded ofloxacin from 8 mV to -15 mV (Fig. 1E). The change of charge indirectly reflected the successful synthesis of OHH NPs. The UV-vis absorption spectra of HMPB NPs, ofloxacin and OHH NPs are shown in Fig. 1F. The as-obtained HMPB NPs possessed a broad absorption in the NIR region with an absorption peak at approximately 710 nm. After loading ofloxacin, a strong absorption peak of OHH NPs appeared at 288 nm which was a characteristic absorption of ofloxacin, indicating that ofloxacin was successfully loaded into HMPB NPs. After coating with HA, the strong absorption peak of OHH NPs red-shifted to 800 nm because of the absorbance of HA. Fig. 1G displayed the FT-IR spectra of HMPB NPs, ofloxacin and OHH NPs. The characteristic peak of HMPB NPs at 2086 cm⁻¹ originated from the -CN stretching vibration. Compared with HMPB NPs, new peaks of OHH NPs appeared at 1414 cm⁻¹, 1708 cm⁻¹ and 1630 cm⁻¹, which was assigned to the C=O, C=C and O-F vibration of ofloxacin, respectively, further demonstrating the successful loading of ofloxacin. Besides, X-ray photoelectron spectroscopy (XPS) was also performed to investigate the chemical composition of OHH NPs. As shown in Fig. 1H, the binding energy peak of HMPB at 708.8 eV was attributed to Fe 2p. However, Fe 2p peak of OHH NPs disappeared due to the presence of HA layer. In addition, obvious binding energy peak located at 689.1 eV corresponding to F 1s was observed from OHH NPs (Fig. S1), indicating successful loading of ofloxacin. The X-ray diffraction (XRD) of OHH NPs showed the same diffraction peak as that of HMPB (Fig. S2), indicating that the crystal structure of HMPB loaded with ofloxacin has no effect. The as-above characterization results solidly demonstrated that OHH NPs was successfully prepared.

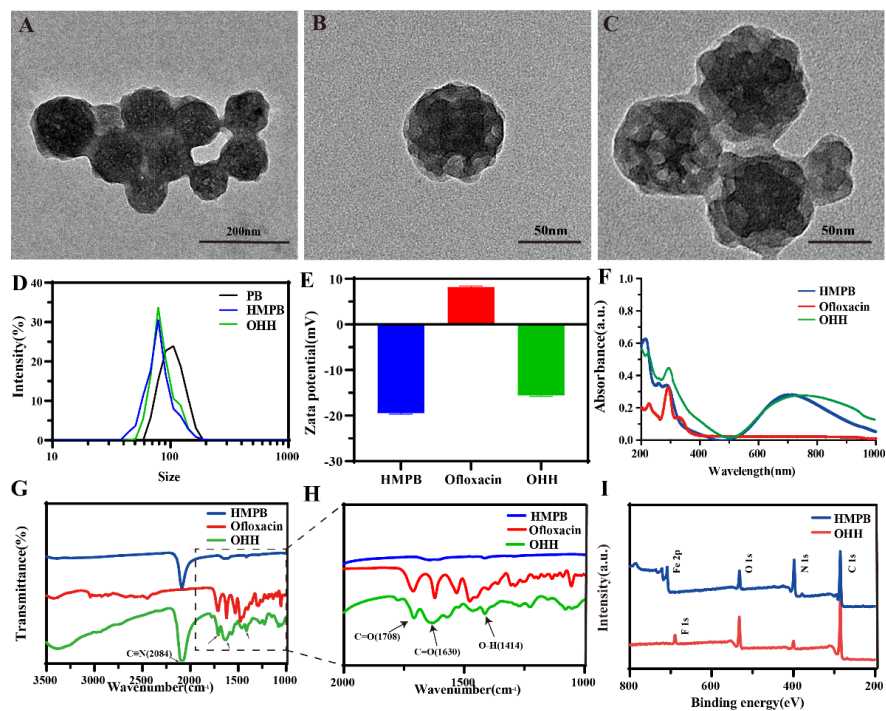


Fig. 1 . Characterization of PB, HMPB and OHH NPs . (A-C)TEM images of PB, HMPB and OHH NPs. (D) Hydrodynamic sizes distribution of PB, HMPB and OHH NPs determined by dynamic light scattering (E) Zeta potentials of PB, HMPB and OHH NPs. (F) UV–Vis spectra of NPs. (G,H) FT-IR spectra of NPs. (I) XPS survey scan of NPs.

3.2. Photothermal effect of OHH NPs

Due to the strong NIR absorption of OHH NPs, the photothermal effect of OHH NPs under an 808 nm NIR light irradiation was systematically assessed.³⁴⁻³⁵ As seen in Fig. 2A, the increased temperature ([?]T) of HMPB NPs and OHH NPs solution was up to 25 °C after irradiation with an 808 nm NIR laser at a power density of 1 W/cm² for 10 min, whereas it was only 4.7 degC and 4.9 degC for pure water and ofloxacin, respectively. The negligible difference of temperature increment between HMPB NPs and OHH NPs suggested that ofloxacin loading and HA modification didn't influence the photothermal property of HMPB NPs. Simultaneously, the real-time photothermal images of Fig. 2B intuitively exhibited the discrepancy of photothermal ability of different nanoparticles. Fig. 2C and Fig. 2D confirmed that the temperature increase of OHH NPs could be precisely tuned by the concentration of OHH NPs and laser intensity. Besides, the previously reported equation³⁷ was used to measure the photothermal conversion efficiency (Fig. 2E). It could be calculated that OHH NPs possessed a relatively high photothermal conversion efficiency of 27.13%. According to five heating-cooling cycles without obvious temperature decrease, it could be concluded that OHH NPs possessed the high photostability stability (Fig. 2F). All the aforementioned results implied that OHH NPs could be utilized to be an excellent photothermal agent for photothermal therapy(PTT).

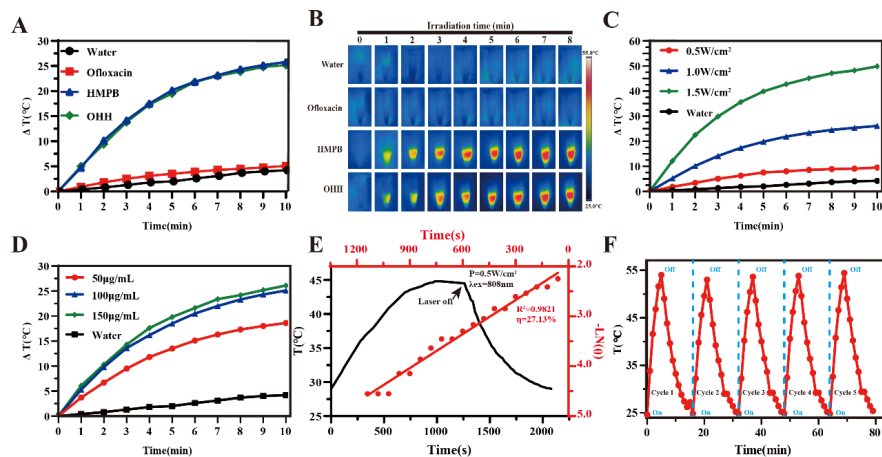


Fig. 2. Photothermal effect of OHH NPs . (A) Photothermal heating curve of water, HMPB, Ofloxacin and OHH NPs. (B) Infrared thermal images of different samples (0.1 mg/mL) irradiated with 808 nm light (1 W/cm², 10 minutes). (C) The heating curve of OHH NPs under different power laser irradiation. (D) Temperature changes of different concentrations of OHH solution irradiated by 808 nm laser. (E) Photothermal effect of OHH NPs under 808 nm laser-on and then laser-off. Plot of linear time data versus $-\ln(\theta)$, which was obtained from the cooling stage (F) Photostability of OHH NPs with 5 cycles.

3.3. Assessment of antibacterial activity

The *in vitro* antibacterial activity of OHH NPs was investigated by bacteriostatic ring test using MRSA and *K.Pneumoniae* as model organisms. After 24 hours of culture, there was not any inhibitory area observed in the tested bacteria after treatment with PBS or HMPB NPs. By contrast, free ofloxacin and OHH NPs treatment groups showed obvious inhibition zone (Fig. 3A) owing to antibacterial activity of ofloxacin. Fig.3B and Fig.3C showed that the diameters of inhibition zones of ofloxacin towards MRSA and *K.Pneumoniae* were \sim 1.70 cm, \sim 3.77 cm, respectively and the diameters of inhibition zones of OHH NPs towards MRSA and *K.Pneumoniae* were \sim 1.48 cm, \sim 3.33 cm, respectively. It should be noted that the inhibition ring of free ofloxacin at an equivalent concentration with loading ofloxacin of OHH NPs was slightly larger than that of OHH NPs, which may be due to slower ofloxacin release of OHH NPs. Meanwhile, the inhibition ring of ofloxacin for *K.Pneumoniae* (Gram-negative bacteria) was much larger than that for MRSA (Gram-positive bacteria), which was attributed to ofloxacin with stronger antibacterial activity towards Gram-negative bacteria. Additionally, the chemo-photothermal synergistic bactericidal efficacy of OHH NPs was investigated using MRSA and *K.Pneumoniae* by the spread plate technique. Specifically, MRSA and *K.Pneumoniae* cells treated with different agents were diluted 10⁵ and 10⁴ times, respectively. In Fig. 3D and 3F, the number of colonies after treatment with NIR or HMPB NPs hardly reduced compared with control group (PBS). However, the significant decrease of the number of bacterial colonies was observed for HMPB NPs+NIR, ofloxacin, ofloxacin+NIR and OHH NPs treated groups. The bacteria-killing efficacy of HMPB NPs+NIR, ofloxacin, ofloxacin+NIR and OHH NPs treated groups reached 28.38%, 53.90%, 49.35% and 27.76% for MRSA, respectively and it reached 51.63%, 75.61%, 73.52% and 72.56% for *K.Pneumoniae*, respectively. These data demonstrated that, in the tested dose range, both sole ofloxacin and photothermal treatment could not eliminate all the bacterial colonies. Surprisingly, the OHH NPs combined with NIR laser (OHH NPs+NIR) exhibited high antibacterial efficiency towards MRSA and *K.Pneumoniae*. Almost no bacterial colonies were observed in OHH NPs+NIR treated groups and the inactivation of bacteria was highly up to 99.99% (Fig. 3E and 3G). The ultrahigh antibacterial efficiency of OHH NPs+NIR could be attributed to the effective synergistic effect of ofloxacin and PTT. Compared with the loading rates of two different Prussian blue (Fig.S3), we can observe that the hollow mesoporous structure can effectively increase the loading of antibiotics. Due to the laser irradiation and the secretion of HAase in bacterial cells, ofloxacin is released from the nanoparticles about 80% for 24 hours.

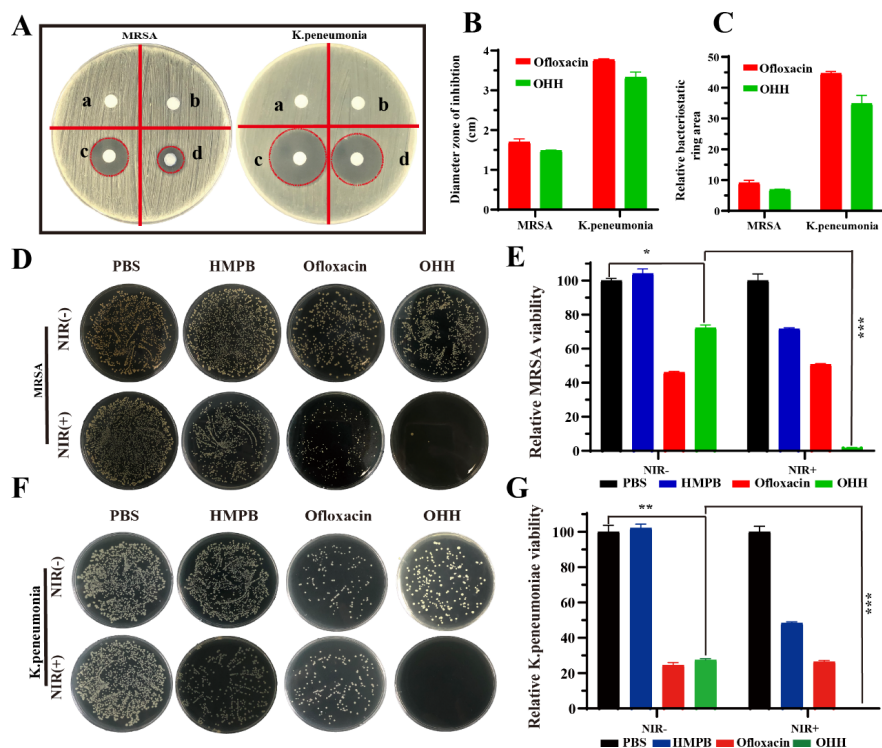


Fig. 3. In vitro antibacterial activity test. (A) Photographs of antibacterial results of PBS(a), HMPB(b), Ofloxacin(c) and OHH NPs(d), against MRSA and *K.pneumoniae*. (B–C) Quantitative measurement of the inhibition zones. (D,F) Photographs of the agar plates of MRSA and Klebsiella Pneumoniae treated with PBS, HMPB, Ofloxacin and OHH NPs with/without 808 nm light irradiation (1 W/cm², 5 min). (E, G) Treatment with PBS was set up as control. Effect of OHH NPs on bacterial counts of MRSA and *K.pneumoniae*. The all concentration above of HMPB is 100 μg/mL and ofloxacin is 10 μg/mL.

Next, the viability of *K.pneumoniae* was further investigated by a fluorescence staining assay based on the integrity of bacterial membrane with HMPB, Ofloxacin and OHH at the same antibiotic concentration (10 μg/mL) and the same HMPB concentration (100 μg/mL). As shown as Fig. 4A, almost no visible red fluorescence was observed after treatment with PBS, NIR and HMPB, indicating nearly all of the bacteria survived in these groups. In comparison, the bacteria treated with HMPB NPs+NIR, ofloxacin, ofloxacin+NIR and OHH NPs+NIR emitted visible red fluorescence, which demonstrated a part of bacteria were killed. However, the bacteria treated by OHH NPs+NIR presented the strongest red fluorescence (Fig. 4B), suggesting most of the bacteria were inactive³⁸. Additionally, SEM images of Fig. 4C further verified that sole PBS and HMPB NPs had no antibacterial ability, which was confirmed by the intact and smooth bacterial membranes, while the bacterial membranes after treatment with OHH NPs+NIR were obviously shrinking. Collectively, all of the results provided confirmative evidence of OHH NPs having highest bacteria-killing ability.

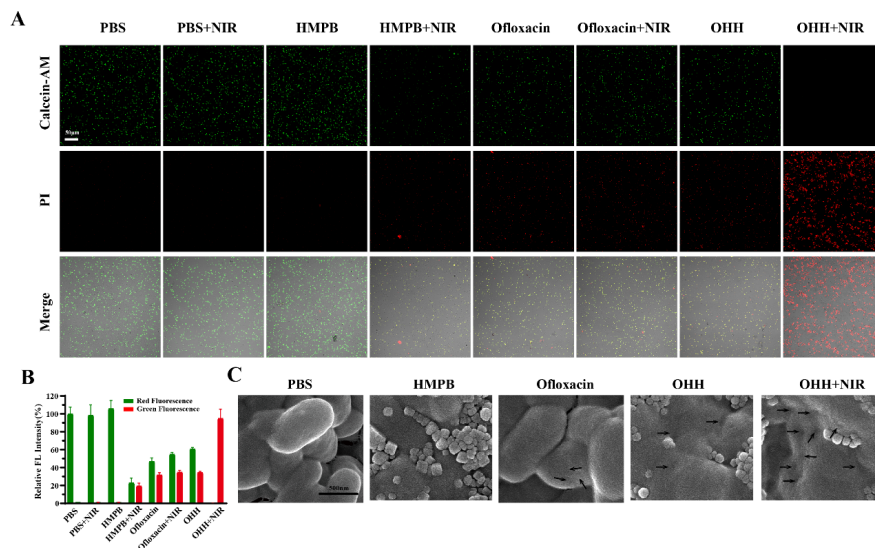


Fig. 4. Observation of bacterial cell wall destruction of *K.pneumoniae*. (A) Calcein-AM/PI staining of *K.pneumoniae* (1×10^8 CFU mL⁻¹) after various treatments. (normal saline, NIR, HMPB, HMPB + NIR, Ofloxacin, Ofloxacin + NIR, OHH NPs, OHH NPs + NIR). The net concentration of the HMPB substrate in all sample groups has been maintained at 100 μ g/mL. (B) The corresponding quantitative analysis of fluorescence intensity by Image J. (C) SEM images of *K.pneumoniae* cells after various treatments.

3.4. Antibacterial mechanism exploration

In addition to the aforementioned results, the antibacterial mechanism was further explored by employing DCFH-DA probe to monitor ROS generation with different treatments on *K.pneumoniae*^{34, 39}. As shown in Fig. 5A and Fig. 5B, the bacteria treated by OHH NPs + NIR exhibited the strongest green fluorescence signal, indicating the highest level of ROS produced, which was likely responsible for the bactericidal efficiency. As the major energy storage molecule, ATP plays a critical role in the various processes of physiology and pathology. Usually, ATP will decrease under conditions of necrosis or apoptosis^{34, 40-42}. We thus wish to explore if the decrease of the ATP level occurs after exposure to OHH NPs+NIR. Fig. 5C showed HMPB NPs treatment hardly caused the decline of ATP level in *K.pneumoniae* comparing with the control group. By comparison, a weak decrease of ATP level was caused after incubation with ofloxacin or OHH NPs. In contrast, ATP level dramatically declined about 92.3% after the treatment of OHH NPs+NIR, suggesting the best antibacterial efficacy of this strategy. Furthermore, protein leakage from *K.pneumoniae* was also investigated, which was taken as a representative indicator of cell membrane damage⁴³. According to Fig. 5D, protein leakage from *K.pneumoniae* of HMPB NPs-treated group was 10.07 μ g/mL, which was similar with the control group. In comparison, protein leakage of bacteria after exposure to ofloxacin and OHH NPs increased to 24.97 μ g/mL and 22.06 μ g/mL, respectively. Notably, protein leakage in the OHH NPs+NIR-treated group was up to 42.26 μ g/mL, which was about 5-fold that of the control group. These results indicated that the combination of ofloxacin and PTT could severely destruct bacterial cell membranes.

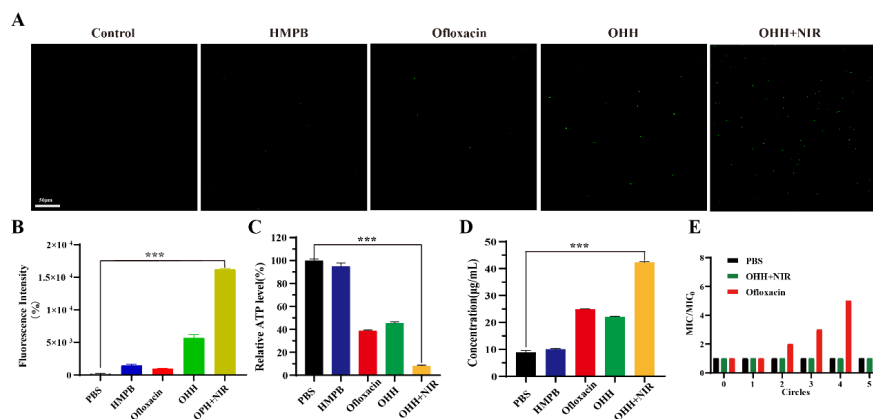


Fig. 5. Antibacterial mechanism investigation . (A) Representative CLSM images to assess intracellular ROS generation in *K.pneumoniae* cells. The samples included normal saline, HMPB(100 µg/mL), Ofloxacin(10 µg/mL), OHH NPs(100 µg/mL) and OHH NPs + NIR (100 µg/mL) (B) The corresponding statistical histogram showing the relative ROS level with Confocal images. (C) ATP level and (D) protein leakage of the *K.pneumoniae* suspensions treated with different group. (E) Drug resistance development profiles of *K.pneumoniae* during serial passaging in the presence of sub-MIC dosing of PBS, Ofloxacin, and OHH NPs. The y-axis indicates the folds of increased MIC compared to the initial ones.

3.5 Drug resistance evaluation

Long-term overuse of antibiotics could easily induce drug resistance of bacteria. Thus, we further explored whether OHH NPs with laser assistance could reduce the occurrence of ofloxacin resistance. To evaluate the development of bacterial resistance with different treatments, *K.pneumoniae* was continuously cultured with a sublethal dose of ofloxacin (one-tenth of the concentration in Fig. 3A) or OHH NPs+NIR. As shown in Fig. 5E, the MIC value of *K.pneumoniae* incubated with ofloxacin was 7 times that of initial MIC after 5 circles' incubation, suggesting serious drug resistance. On the contrary, the MIC value of *K.pneumoniae* after 5 circles' treatment with OHH NPs+NIR was nearly same as the initial MIC. Due to the effective synergy of OHH NPs and PTT, OHH NPs showed excellent antibacterial ability with laser assistance. Therefore, OHH NPs combined with laser irradiation could effectively reduce the dosage of ofloxacin without compromising the bactericidal capability and delay the development of drug resistance, which could be considered as a long-term antibacterial strategy.

3.6. In vitro dispersion of established *K.pneumoniae* biofilms

Over 60% of all patients' infections treated by physicians are caused by biofilms which are of great significance for bacterial attachment and proliferation, and extremely recalcitrant to antimicrobials⁴⁴⁻⁴⁵. Thus, we further studied the potential influence for formed *K.pneumoniae* biofilms mediated by OHH NPs +NIR. As seen in Fig. 6A, comparing with the control group, separate HMPB NPs treatment hardly showed dispersion effect on the biofilms. In comparison, ofloxacin and OHH NPs were able to only remove about 35% and 26% of the biofilm, respectively, indicating that ofloxacin showed certain effectiveness in anti-biofilm (Fig. 6B). However, OHH NPs with laser assistance effectively eliminated the biofilm quantity of 90%, which was likely due to the excellent synergistic effect of ofloxacin and photothermal ablation. We next performed a fluorescence staining assay using PI to obtain 3D CLSM images of *K.pneumoniae* biofilms. It could be concluded that OHH NPs with NIR irradiation exhibited most powerful anti-biofilms activity from the strongest red fluorescence in Fig. 6C and Fig. 6D, which was well consistent with the crystal violet staining assay.

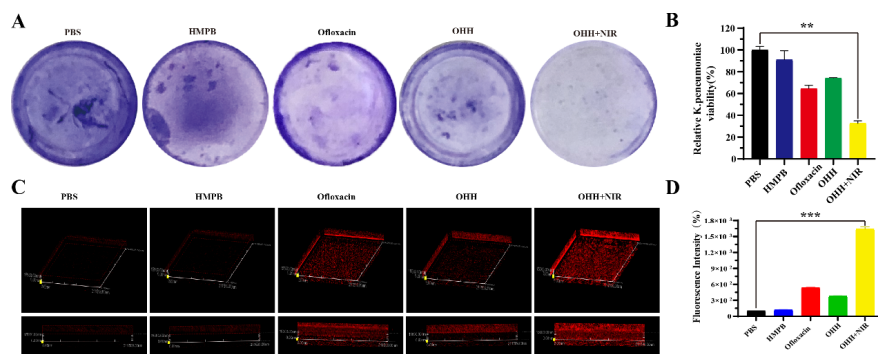


Fig. 6. In vitro anti-biofilms effect of OHH NPs. The remaining biofilms were quantified by crystal violet staining. Biofilms were visualized by photographs (A) and biofilm biomass was determined by measuring the absorbance of 590 nm. (B). (C) Confocal fluorescence images of *K. pneumoniae* biofilms. (D) The corresponding statistical histogram showing the relative biofilm level. The group was used as the PBS, HMPB NPs (100 $\mu\text{g}/\text{mL}$), ofloxacin (10 $\mu\text{g}/\text{mL}$), OHH NPs (100 $\mu\text{g}/\text{mL}$) and OHH NPs + NIR (100 $\mu\text{g}/\text{mL}$).

3.7. In vitro cytotoxicity study

The biocompatibility of agents is the most important precondition of clinical translation. To make sure that OHH NPs could be potentially translated for practical application, *in vitro* cytotoxicity experiments were performed with NIH-3T3 cells and HUV-EC cells. According to Fig. 7A and Fig. S5, the viability of two cell lines incubated with various concentrations of OHH NPs for 24 h remained at 100%, even at the concentration of 125 $\mu\text{g}/\text{mL}$, suggesting the ultra-low cytotoxic nature of OHH NPs. The *in vitro* biocompatibility of OHH NPs was further assessed by hemolysis assay. As can be seen in Fig. 7B, hemolytic rate after exposure to OHH NPs even at the concentration of 150 $\mu\text{g}/\text{mL}$ was only 3.9%, indicating good biocompatibility of OHH NPs. In hemolysis and cytotoxicity assays (Fig. S6), it should be noted that OHH NPs showed better biocompatibility than HMPB NPs, which was likely attributed to the fact that HA coating with superior biocompatibility reduced *in vitro* cytotoxicity of HMPB NPs. In addition, platelet aggregation assay displayed OHH NPs hardly caused platelet aggregation, demonstrating their little risk of inducing thrombosis (Fig. S7).

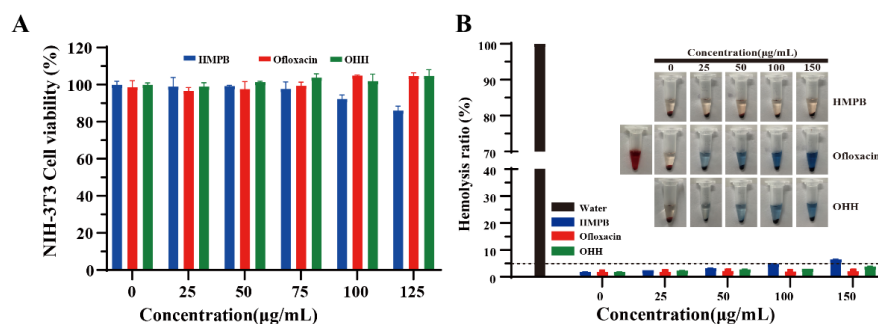


Fig. 7 In vitro biosafety of nanomaterials . (A) Cell viability and (B) hemolysis assays of HMPB, Ofloxacin, OHH NPs with different concentrations.

3.8. In vivo evaluation of wound healing

We also evaluated the *in vivo* healing ability of mice with a *K. pneumoniae* -infected wound utilizing the synergistic antibacterial strategy. Female BALB/c mice with *K. pneumoniae* -infected wound on their back were used as a model for the study (Fig. 8A). Fig. 8B displayed representative photographs of wound healing after different treatments at different time points. And traces of wound closure for 12 days for all treatment

groups were also drawn (Fig. 8C). We observed that OHH NPs+NIR is almost healed. On day 12, the size of infected wounds after treatment with PBS, HMPB NPs, ofloxacin, OHH NPs and OHH NPs+NIR reduced to 35.51%, 33.94%, 36.82%, 36.54%, 17.53%, of the original wound area, respectively, indicating the superiority of combination therapy for infected wound healing (Fig. 8D). Moreover, the insignificant body weight change of mice demonstrated all treatment groups with the low toxicity (Fig. 8E). In addition, the *in vivo* antibacterial effect of all treatment groups was also assessed. As shown in Fig. 8F and 8G, the combination of OHH NPs and PTT exhibited best antibacterial effect for *K.pneumoniae* -infected wound comparing with all single-mode therapies, which was in accord with the *in vitro* antibacterial test in Fig. 3. Besides, the temperature of the wound region treated with OHH NPs increased to $\sim 52^{\circ}\text{C}$ after irradiation for 5 min, the temperature of group PBS did not change significantly. (Fig. S8).

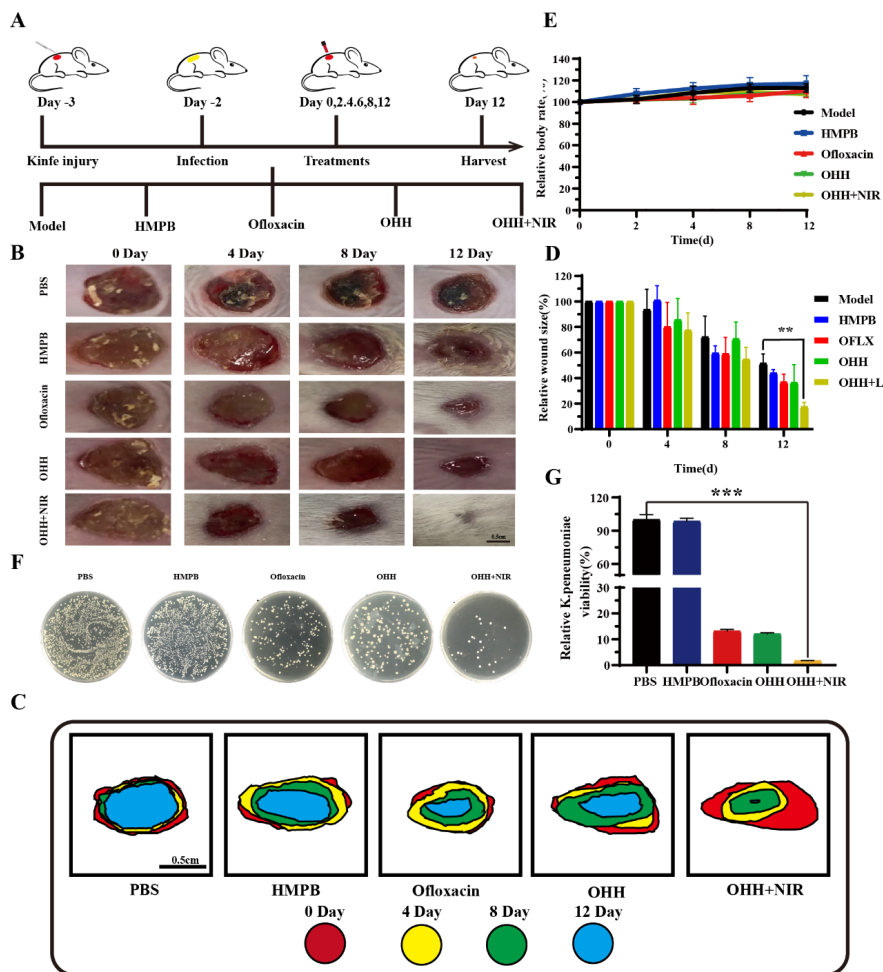


Fig. 8. Macroscopic evaluation and histological analysis of wound models in vivo. (A) Scheme for in vivo test including the establishment of *K.pneumoniae* infection model and subsequent treatment regime. (B) Changes in mice body weight during the treatment. (C) Representative photographs of wounds at day 0, 4, 8, and 12 and (D) wound closure rates. (E) Representative photographs of bacteria colonies derived from the infected sites of mice with different treatment as indicated. (F) Corresponding quantitative data of bacterial colonies in (E). (G) Wound area traces of each group during 12 days.

The wound closure efficacy after different treatments was also assessed by performing histological analysis of wound tissues. As shown in Fig. 9A, mass inflammatory cells were observed in PBS, HMPB, Ofloxacin, and

OHH NPs groups, suggesting the wound recovery was incomplete. However, the wounds of OHH NPs+NIR showed almost as complete as normal tissue without obvious inflammation. Furthermore, the collagen deposition of wound area was investigated by Masson's trichrome staining. Fig. 9B showed the regenerated collagen fiber stained with blue color in OHH NPs+NIR-treated group was continuous and more obvious than that in other treated groups, which reflected better recovery of combination therapy. All of the results confirmed the best healing efficiency of OHH NPs+NIR strategy.

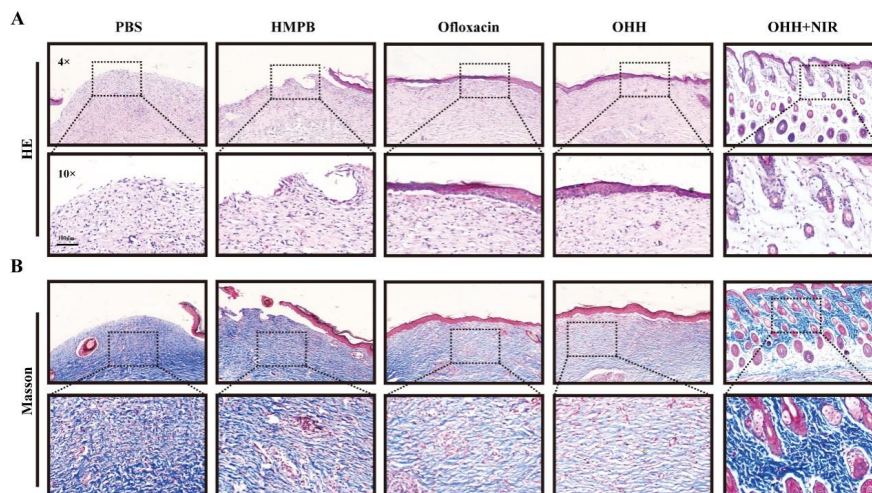


Fig. 9. Histologic analysis of infected tissues after 12 days of treatments . (A) HE staining;(B) Masson staining.

3.9. In vivo biological safety study

In order to evaluate the in vivo potential toxicity of OHH NPs+NIR, biochemical analysis of all mice with different treatments was performed when wound healing experiment was completed. Fig. 10A-D showed that there were no obvious differences among all groups in total white blood cell (WBC), total red blood cells (RBC), hemoglobin (HGB) and blood platelet (PLT) counts. Meanwhile, no abnormalities were found in key functional hepatic and kidney indicators, such as ALT, AST, UREA and CREA (Fig. 10E-H). In addition, H&E staining images of the major organs including heart, liver, spleen, kidney, and lung confirmed normal tissue structures without any visible organ damage. All these results strongly demonstrated our developed therapeutic strategy of OHH NPs+NIR with the superior biosafety for in vivo infected wound healing therapy.

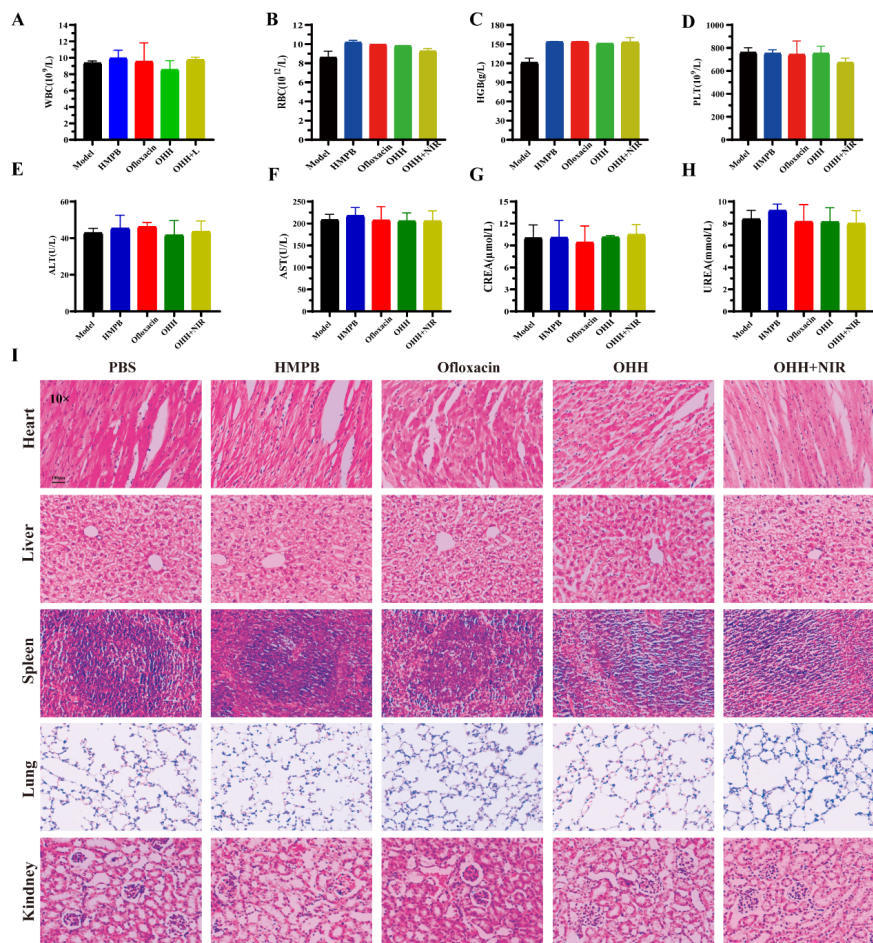


Fig. 10. Toxicity evaluation of nanoparticles in vivo. (A-D) Blood biochemistry data WBC, RBC, HGB and PLT (E-H) Blood biochemistry data including liver and kidney function markers: ALT, AST, UREA and CREA. (I) Representative H&E stained slices of major organs.

4. Conclusion

In summary, the OHH NPs nanoplatform was fabricated for antibiotic-photothermal ablation of *K.pneumoniae* bacteria. The integrated nanoplatform could efficiently adhere onto *K.pneumoniae* bacteria and damage bacterial membrane by subsequent PTT under NIR irradiation. The exploration of the antibacterial mechanism shows that the powerful bactericidal ability of the cooperative system and the inhibition of drug resistance can be attributed to the generation of ROS, which destroys the integrity of cell membranes, reduces ATP and disrupts bacterial metabolism. The outstanding bactericidal capability of the OHH NPs nanoplatform under NIR irradiation was also confirmed by an in vivo *K.pneumoniae* -infected model on mice. OHH NPs nanoplatform combined with antibiotic-photothermal therapy can be considered as a very promising strategy to effectively eliminate bacteria and inhibit the development of drug resistance.

Acknowledgement

This work was partially supported by the Natural Science Foundation of Hunan Province (2020JJ4005, 2021JJ3016), the Opening Foundation of Key Laboratory of Study and Discovery of Small Targeted Molecules of Hunan Province(2019CG03), the Opening Foundation of School of Medicine, Hunan Normal University(KF2021023).

Conflicts of interest

The authors declare that they have no conflict of interest.

References

- (1) Taubes, G., The Bacteria Fight Back. *Science* **2008**, *321* (5887), 356-361.
- (2) Levy, S. B.; Marshall, B., Antibacterial resistance worldwide: causes, challenges and responses. *Nat Med* **2004**, *10* (12 Suppl), S122-9.
- (3) Hartmann, M.; Betz, P.; Sun, Y.; Gorb, S. N.; Lindhorst, T. K.; Krueger, A., Saccharide-modified nanodiamond conjugates for the efficient detection and removal of pathogenic bacteria. *Chemistry* **2012**, *18* (21), 6485-92.
- (4) Kieron; M.; G.; O'Connell; James; T.; Hodgkinson; Hannah; F.; Sore, Combating Multidrug-Resistant Bacteria: Current Strategies for the Discovery of Novel Antibacterials. *Angewandte Chemie International Edition* **2013**, *52* (41), 10706-10733.
- (5) Morgan, D.; Okeke, I. N.; Laxminarayan, R.; Perencevich, E. N.; Weisenberg, S., Non-prescription antimicrobial use worldwide: a systematic review. *Lancet Infectious Diseases* **2011**, *11* (9), 692-701.
- (6) Michaelidou, M.; Karageorgos, S. A.; Tsioutis, C., Antibiotic Use and Antibiotic Resistance: Public Awareness Survey in the Republic of Cyprus. *Antibiotics (Basel)* **2020**, *9* (11).
- (7) Qing, G.; Zhao, X.; Gong, N.; Chen, J.; Liang, X. J., Thermo-responsive triple-function nanotransporter for efficient chemo-photothermal therapy of multidrug-resistant bacterial infection. *Nature Communications* **2019**, *10* (1), 1-12.
- (8) Sun, P.; Zhang, Y.; Ran, X.; Liu, C.; Wang, Z.; Ren, J.; Qu, X., Phytochemical-encapsulated nanoplat-form for “on-demand” synergistic treatment of multidrug-resistant bacteria. *Nano Research* **2018**, *11* (7), 3762-3770.
- (9) Zhang, Y.; Sun, P.; Zhang, L.; Wang, Z.; Wang, F.; Dong, K.; Liu, Z.; Ren, J.; Qu, X., Silver-Infused Porphyrinic Metal-Organic Framework: Surface-Adaptive, On-Demand Nanoplat-form for Synergistic Bacteria Killing and Wound Disinfection. *Advanced Functional Materials* **2019**, *29* (11).
- (10) Wang, Y.; Ding, X.; Chen, Y.; Guo, M.; Zhang, Y.; Guo, X.; Gu, H., Antibiotic-loaded, silver core-embedded mesoporous silica nanovehicles as a synergistic antibacterial agent for the treatment of drug-resistant infections. *Biomaterials* **2016**, *101* , 207-216.
- (11) Gao, G.; Jiang, Y. W.; Jia, H. R.; Wu, F. G., Near-infrared light-controllable on-demand antibiotics release using thermo-sensitive hydrogel-based drug reservoir for combating bacterial infection. *Biomaterials* **2019**, *188* , 83-95.
- (12) Wu, Y.; Song, Z.; Wang, H.; Han, H., Endogenous stimulus-powered antibiotic release from nanoreactors for a combination therapy of bacterial infections. *Nat Commun* **2019**, *10* (1), 4464.
- (13) Tao, B.; Lin, C.; Yuan, Z.; He, Y.; Cai, K., Near infrared light-triggered on-demand Cur release from Gel-PDA@Cur composite hydrogel for antibacterial wound healing. *Chemical Engineering Journal* **2020**, *403* , 126182.
- (14) Zhao, Y.; Dai, X.; Wei, X.; Yu, Y.; Chen, X.; Zhang, X.; Li, C., Near-Infrared Light-Activated Thermosensitive Liposomes as Efficient Agents for Photothermal and Antibiotic Synergistic Therapy of Bacterial Biofilm. *ACS Appl Mater Interfaces* **2018**, *10* (17), 14426-14437.
- (15) J. Ouyang, R. Y. L., W. Chen, Z. Liu, Q. Xu, K. Zeng, L. Deng, L. Shen, Y.N. Liu., A black phosphorus based synergistic antibacterial platform against drug resistant bacteria. *J. Mater. Chem. B* **2018**, *6* , 6302-6310.

- (16) Wang X, S. K., Tan L, Liu X, Cui Z, Jing D, Yang X, Liang Y, Li Z, Zhu S, Yeung KWK, Zheng D, Wu S, Rapid and highly effective noninvasive disinfection by hybrid Ag/CS@MnO₂ nanosheets using near-infrared light[J]. *ACS Appl. Mater. Interfaces* **2019**, *11* (16), 15014-15027.
- (17) Yang, Y.; He, P.; Wang, Y.; Bai, H.; Wang, S.; Xu, J.-F.; Zhang, X., Supramolecular Radical Anions Triggered by Bacteria In Situ for Selective Photothermal Therapy. *Angewandte Chemie International Edition* **2017**, *56* (51), 16239-16242.
- (18) Gao, Q.; Zhang, X.; Yin, W.; Ma, D.; Xie, C.; Zheng, L.; Dong, X.; Mei, L.; Yu, J.; Wang, C.; Gu, Z.; Zhao, Y., Functionalized MoS₂ Nanovehicle with Near-Infrared Laser-Mediated Nitric Oxide Release and Photothermal Activities for Advanced Bacteria-Infected Wound Therapy. *Small* **2018**, *14* (45), 1802290.
- (19) Yang, Y.; Ma, L.; Cheng, C.; Deng, Y.; Huang, J.; Fan, X.; Nie, C.; Zhao, W.; Zhao, C., Nonchemotherapeutic and Robust Dual-Responsive Nanoagents with On-Demand Bacterial Trapping, Ablation, and Release for Efficient Wound Disinfection. *Advanced Functional Materials* **2018**, *28* (21), 1705708.
- (20) Hu, D.; Li, H.; Wang, B.; Ye, Z.; Lei, W.; Jia, F.; Jin, Q.; Ren, K.-F.; Ji, J., Surface-Adaptive Gold Nanoparticles with Effective Adherence and Enhanced Photothermal Ablation of Methicillin-Resistant Staphylococcus aureus Biofilm. *ACS Nano* **2017**, *11* (9), 9330-9339.
- (21) Ray, P. C.; Khan, S. A.; Singh, A. K.; Senapati, D.; Fan, Z., Nanomaterials for targeted detection and photothermal killing of bacteria. *Chemical Society Reviews* **2012**, *41* (8), 3193.
- (22) Gao, Q.; Zhang, X.; Yin, W.; Ma, D.; Xie, C.; Zheng, L.; Dong, X.; Mei, L.; Yu, J.; Wang, C.; Gu, Z.; Zhao, Y., Functionalized MoS₂ Nanovehicle with Near-Infrared Laser-Mediated Nitric Oxide Release and Photothermal Activities for Advanced Bacteria-Infected Wound Therapy. *Small* **2018**, *14* (45), e1802290.
- (23) Yuwen, L.; Sun, Y.; Tan, G.; Xiu, W.; Zhang, Y.; Weng, L.; Teng, Z.; Wang, L., MoS₂@polydopamine-Ag nanosheets with enhanced antibacterial activity for effective treatment of Staphylococcus aureus biofilms and wound infection. *Nanoscale* **2018**, *10*(35), 16711-16720.
- (24) J. Sun, L. S., Y. Fan, L. Tian, S. Luan, S. Niu, L. Ren, W. Ming, J. Zhao, Synergistic photodynamic and photothermal antibacterial nanocomposite membrane triggered by single NIR light source. *ACS Appl Mater Interfaces* **2019**, *11* (30), 26581-26589.
- (25) Rubio-Ruiz, B.; Perez-Lopez, A. M.; Bray, T. L.; Lee, M.; Serrels, A.; Prieto, M.; Arruebo, M.; Carragher, N. O.; Sebastian, V.; Unciti-Broceta, A., High-Precision Photothermal Ablation Using Biocompatible Palladium Nanoparticles and Laser Scanning Microscopy. *ACS Appl Mater Interfaces* **2018**, *10* (4), 3341-3348.
- (26) Wang, H.; Zhao, B.; Dong, W.; Zhong, Y.; Zhang, X.; Gong, Y.; Zhan, R.; Xing, M.; Zhang, J.; Luo, G.; Qian, W., A dual-targeted platform based on graphene for synergistic chemo-photothermal therapy against multidrug-resistant Gram-negative bacteria and their biofilms. *Chemical Engineering Journal* **2020**, *393* , 124595.
- (27) Zeng, X.; Luo, M.; Liu, G.; Wang, X.; Tao, W.; Lin, Y.; Ji, X.; Nie, L.; Mei, L., Polydopamine-Modified Black Phosphorous Nanocapsule with Enhanced Stability and Photothermal Performance for Tumor Multimodal Treatments. *Advanced science* **2018**, *5*(10), 1800510.
- (28) Mei, Z.; Gao, D.; Hu, D.; Zhou, H.; Ma, T.; Huang, L.; Liu, X.; Zheng, R.; Zheng, H.; Zhao, P.; Zhou, J.; Sheng, Z., Activatable NIR-II photoacoustic imaging and photochemical synergistic therapy of MRSA infections using miniature Au/Ag nanorods. *Biomaterials* **2020**, *251* , 120092.
- (29) C. Tong, X. Z., Y. Yang, X. Liu, G. Zhong, C. Xiao, B. Liu, W. Wang, X. Yang, PB@PDA@Ag nanosystem for synergistically eradicating MRSA and accelerating diabetic wound healing assisted with laser irradiation. *Biomaterials* **2020**, *243* , 119936.

- (30) Liu B, W. W., Fan J, Long Y, Xiao F, et al, RBC membrane camouflaged prussian blue nanoparticles for gamabutolin loading and combined chemo/photothermal therapy of breast cancer. *Biomaterials* **217** , 119301.
- (31) Cai, X.; Jia, X.; Gao, W.; Zhang, K.; Ma, M.; Wang, S.; Zheng, Y.; Shi, J.; Chen, H., A Versatile Nanotheranostic Agent for Efficient Dual-Mode Imaging Guided Synergistic Chemo-Thermal Tumor Therapy. *Advanced Functional Materials* **2015**, *25* (17), 2520-2529.
- (32) Zhou, J.; Li, M.; Hou, Y.; Luo, Z.; Chen, Q.; Cao, H.; Huo, R.; Xue, C.; Sutrisno, L.; Hao, L.; Cao, Y.; Ran, H.; Lu, L.; Li, K.; Cai, K., Engineering of a Nanosized Biocatalyst for Combined Tumor Starvation and Low-Temperature Photothermal Therapy. *ACS Nano* **2018**, *12* (3), 2858-2872.
- (33) Fan, J.; Liu, B.; Long, Y.; Wang, Z.; Tong, C.; Wang, W.; You, P.; Liu, X., Sequentially-targeted biomimetic nano drug system for triple-negative breast cancer ablation and lung metastasis inhibition. *Acta Biomater* **2020**, *113* , 554-569.
- (34) Tong, C.; Zhong, X.; Yang, Y.; Liu, X.; Zhong, G.; Xiao, C.; Liu, B.; Wang, W.; Yang, X., PB@PDA@Ag nanosystem for synergistically eradicating MRSA and accelerating diabetic wound healing assisted with laser irradiation. *Biomaterials* **2020**, *243* , 119936.
- (35) Liu, B.; Wang, W.; Fan, J.; Long, Y.; Xiao, F.; Daniyal, M.; Tong, C.; Xie, Q.; Jian, Y.; Li, B.; Ma, X.; Wang, W., RBC membrane camouflaged prussian blue nanoparticles for gamabutolin loading and combined chemo/photothermal therapy of breast cancer. *Biomaterials* **2019**, *217* , 119301.
- (36) Xiao, F.; Fan, J.; Tong, C.; Xiao, C.; Wang, Z.; Liu, B.; Daniyal, M.; Wang, W., An erythrocyte membrane coated mimetic nano-platform for chemo-phototherapy and multimodal imaging. *RSC Advances* **2019**, *9* (48), 27911-27926.
- (37) Zhong, X.; Tong, C.; Liu, T.; Li, L.; Liu, X.; Yang, Y.; Liu, R.; Liu, B., Silver nanoparticles coated by green graphene quantum dots for accelerating the healing of MRSA-infected wounds. *Biomaterials Science* **2020**, *8* (23), 6670-6682.
- (38) Wang, L.; Yang, J.; Yang, X.; Hou, Q.; Liu, S.; Zheng, W.; Long, Y.; Jiang, X., Mercaptophenylboronic Acid-Activated Gold Nanoparticles as Nanoantibiotics against Multidrug-Resistant Bacteria. *ACS Appl Mater Interfaces* **2020**, *12* (46), 51148-51159.
- (39) Li, Y.; Gao, Z.; Zhang, Y.; Chen, F.; An, P.; Wu, H.; You, C.; Sun, B., MOF-shielded and glucose-responsive ultrasmall silver nano-factory for highly-efficient anticancer and antibacterial therapy. *Chemical Engineering Journal* **2021**, *416* , 127610.
- (40) Tong, C.; Li, L.; Xiao, F.; Fan, J.; Zhong, X.; Liu, X.; Liu, B.; Wu, Z.; Zhou, J., Daptomycin and AgNP co-loaded rGO nanocomposites for specific treatment of Gram-positive bacterial infection in vitro and in vivo. *Biomaterials Science* **2019**, *7* (12), 5097-5111.
- (41) Tong, C.; Zou, W.; Ning, W.; Fan, J.; Li, L.; Liu, B.; Liu, X., Synthesis of DNA-guided silver nanoparticles on a graphene oxide surface: enhancing the antibacterial effect and the wound healing activity. *RSC Advances* **2018**, *8* (49), 28238-28248.
- (42) Cui, Y.; Zhao, Y.; Tian, Y.; Zhang, W.; Lu, X.; Jiang, X., The molecular mechanism of action of bactericidal gold nanoparticles on Escherichia coli. *Biomaterials* **2012**, *33* (7), 2327-33.
- (43) Zhao, R.; Kong, W.; Sun, M.; Yang, Y.; Liu, W.; Lv, M.; Song, S.; Wang, L.; Song, H.; Hao, R., Highly Stable Graphene-Based Nanocomposite (GO-PEI-Ag) with Broad-Spectrum, Long-Term Antimicrobial Activity and Antibiofilm Effects. *ACS Appl Mater Interfaces* **2018**, *10* (21), 17617-17629.
- (44) Hu, D.; Zou, L.; Yu, W.; Jia, F.; Han, H.; Yao, K.; Jin, Q.; Ji, J., Relief of Biofilm Hypoxia Using an Oxygen Nanocarrier: A New Paradigm for Enhanced Antibiotic Therapy. *Adv Sci (Weinh)* **2020**, *7* (12), 2000398.

(45) Ivanova, A.; Ivanova, K.; Tied, A.; Heinze, T.; Tzanov, T., Layer-By-Layer Coating of Aminocellulose and Quorum Quenching Acylase on Silver Nanoparticles Synergistically Eradicate Bacteria and Their Biofilms. *Advanced Functional Materials* **2020**, *30*(24).